

This work was written as part of one of the author's official duties as an Employee of the United States Government and is therefore a work of the United States Government. In accordance with 17 U.S.C. 105, no copyright protection is available for such works under U.S. Law. Access to this work was provided by the University of Maryland, Baltimore County (UMBC) ScholarWorks@UMBC digital repository on the Maryland Shared Open Access (MD-SOAR) platform.

Please provide feedback

Please support the ScholarWorks@UMBC repository by emailing scholarworks-group@umbc.edu and telling us what having access to this work means to you and why it's important to you. Thank you.

Supporting Information

Malic Acid Carbon Dots: From Super-resolution Live-Cell Imaging to Highly Efficient Separation

Bo Zhi,^{†,‡} Yi Cui,^{§,‡} Shengyang Wang,[†] Benjamin P. Frank,^Δ Denise N. Williams,[⊥] Richard P. Brown,[⊥] Eric S. Melby,^{§,¶} Robert J. Hamers,^{||} Zeev Rosenzweig,[⊥] D. Howard Fairbrother,^Δ Galya Orr,^{§,*} Christy L. Haynes^{†,*}

[†]Department of Chemistry, University of Minnesota – Twin Cities, MN 55455, USA

[§]Environmental Molecular Sciences Laboratory, Pacific Northwest National Laboratory, WA 99354, USA

^ΔDepartment of Chemistry, The Johns Hopkins University, MD 21218, USA

[⊥]Department of Chemistry and Biochemistry, University of Maryland, Baltimore County, MD 21250, USA

^{||}Department of Chemistry, University of Wisconsin-Madison, WI 53706, USA

*Corresponding authors:

Email: chaynes@umn.edu (Dr. Christy L. Haynes)

Email: galya.orr@pnnl.gov (Dr. Galya Orr)

[‡]These authors contributed equally to this work.

Supporting information list

Figure S1: Evaluation of MACD biocompatibility/cytotoxicity.

Figure S2: Recording of cross-membrane uptake and intracellular transport of MACDs.

Figure S3: Super-resolution imaging of MACDs in live trout epithelial gill cells.

Scheme S1: Illustration of the separation process for as-synthesized MACDs.

Figure S4: Pictures of fractionated MACDs.

Figure S5: Photoluminescence properties of MACD fraction #14 after the 1st separation cycle.

Figure S6: Comparison of particle size distributions (PSDs) determined by TEM.

Figure S7: Dynamic light scattering results (DLS) for MACD fractions.

Figure S8: 3D excitation-emission matrices (EEM) and fluorescence lifetime results for MACD fractions.

Figure S9: 2D excitation emission contour images of MACD fractions.

Table S1: The sequence information of single-molecule fluorescence *in situ* hybridization probes.

Movie S1: Demonstration of the *in vitro* photoblinking of MACDs.

Movie S2: Demonstration of MACD photoblinking in trout gill cells.

Movie S3: Demonstration of MACD uptake by live cells.

Movie S4: Demonstration of MACD transport in live cells.

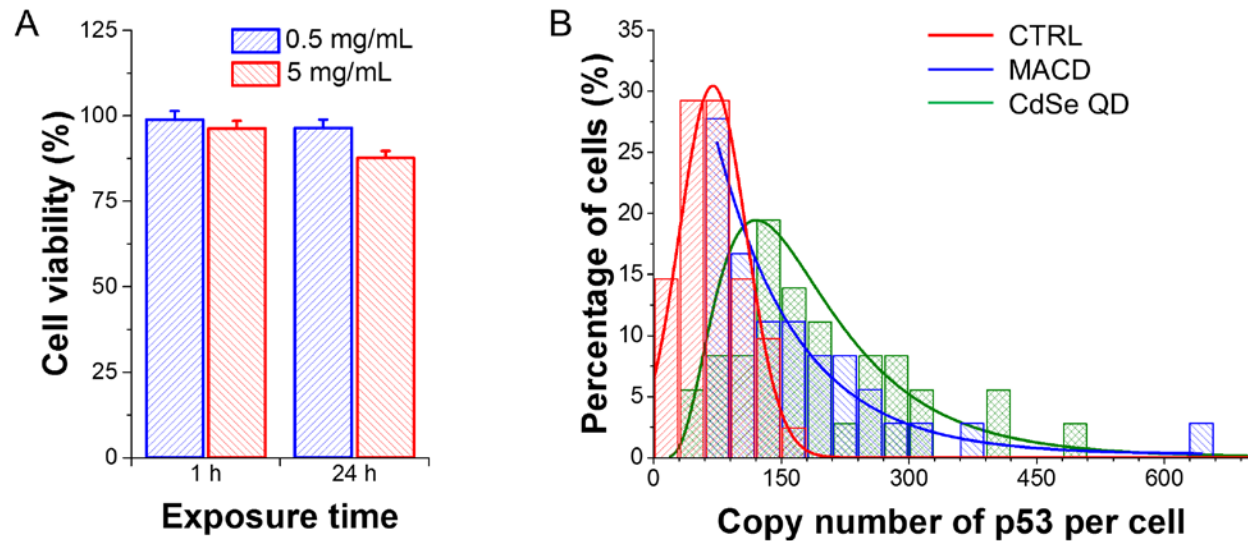


Figure S1. Evaluation of MACD biocompatibility. (A) The impact of MACDs on the trout epithelial gill cell viability was assessed using the MTS assay (error bars indicate the standard deviation of six independent replicates). (B) The impact of MACDs and QDs on the expression of p53 gene was quantified using single molecule fluorescence *in-situ* hybridization (smFISH) in individual cells. The histograms are fitted with lognormal function. ($n > 70$ cells).

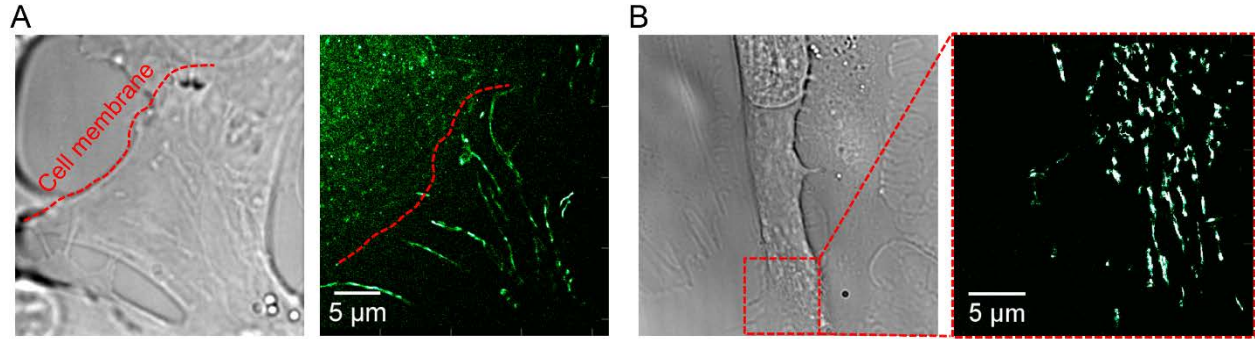


Figure S2. Recording of cross-membrane uptake and intracellular transport of MACDs. (A) Upon internalization, freely diffusing MACDs outside the cell membrane become localized to filamentous structures (corresponding to Movie S3). (B) In the highlighted region, directional movement of MACD containing vesicles is observed, suggesting the involvement of cytoskeletal filaments, possibly microtubules, in the transport of MACDs within or associated with mitochondria (corresponding to Movie S4).

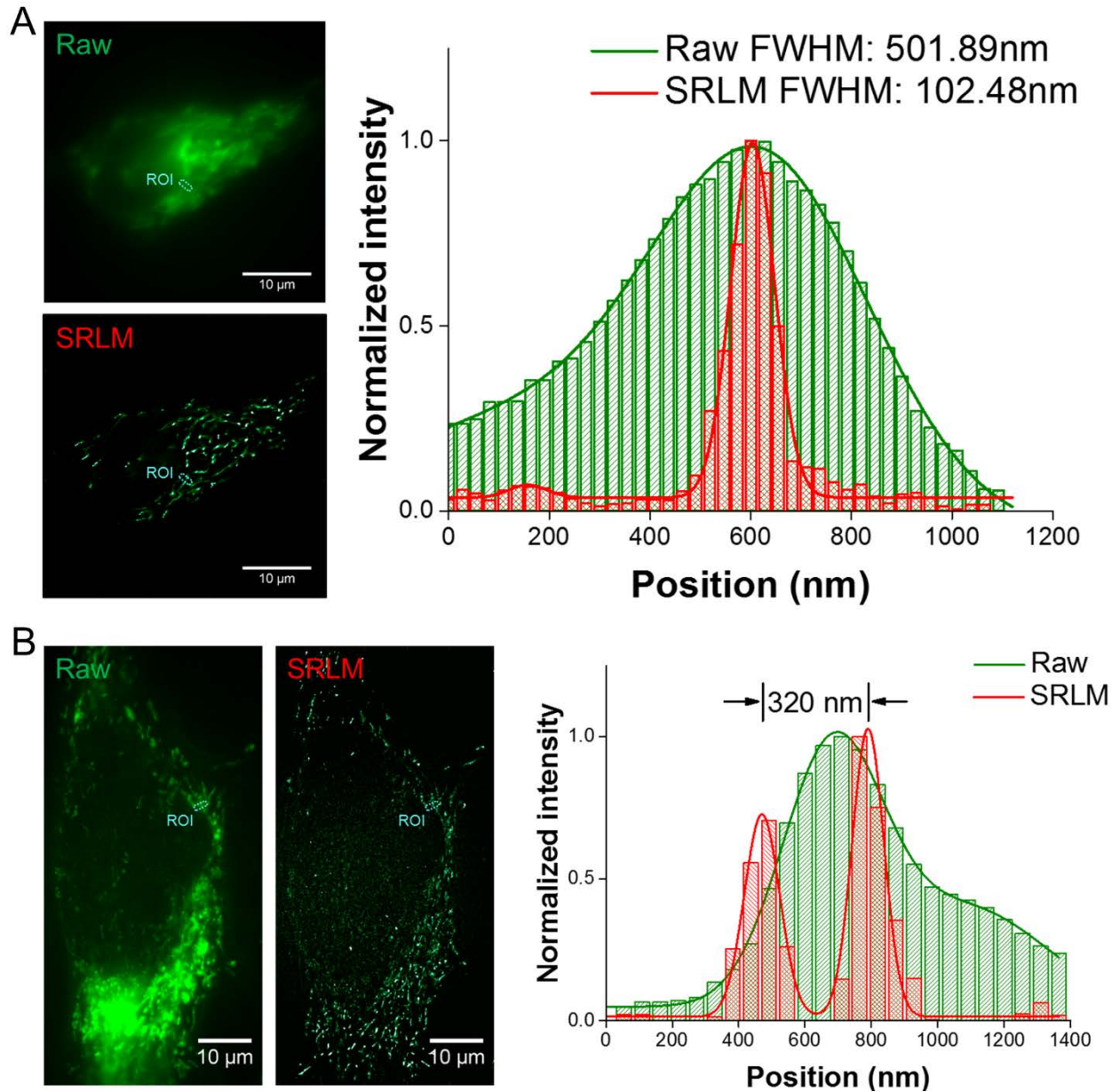
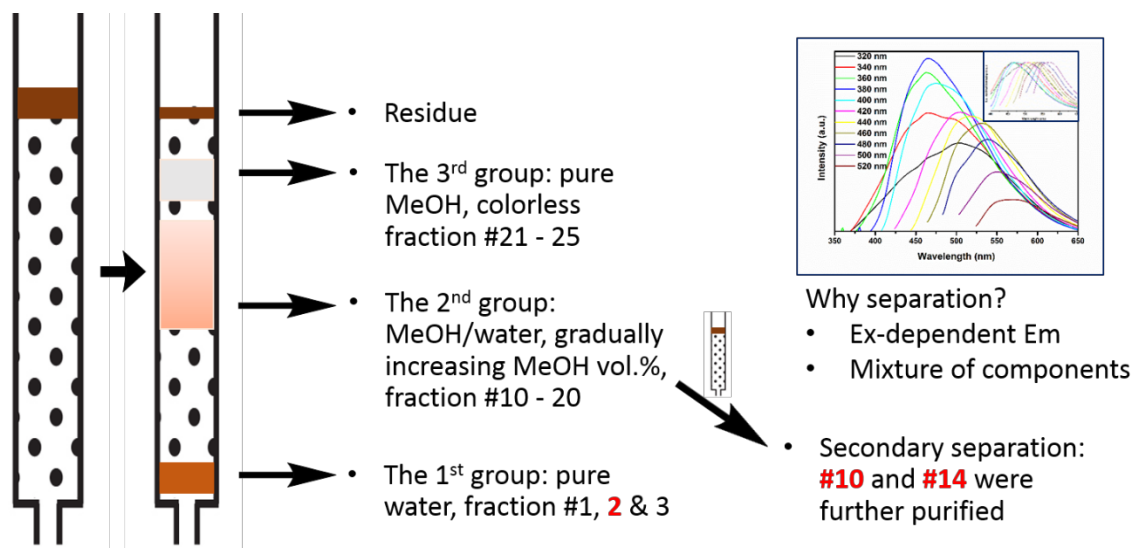


Figure S3. Super-resolution imaging of MACDs in live trout epithelial gill cells. (A) Demonstration and quantification of the enhanced spatial resolution (right panel) for the region of interest (ROI) marked in the fluorescence images. (B) The enhanced ability to distinguish between closely adjacent objects is demonstrated and quantified in the emission profile (right panel) for the ROI marked in the fluorescence images, revealing the two peaks that are hidden in the raw image.



Scheme S1. The general set-up and process of MACD separation by C₁₈ reverse-phased silica gel column chromatography. The inset fluorescence spectra show the remarkable excitation-dependent emission of as-synthesized MACDs before separation.

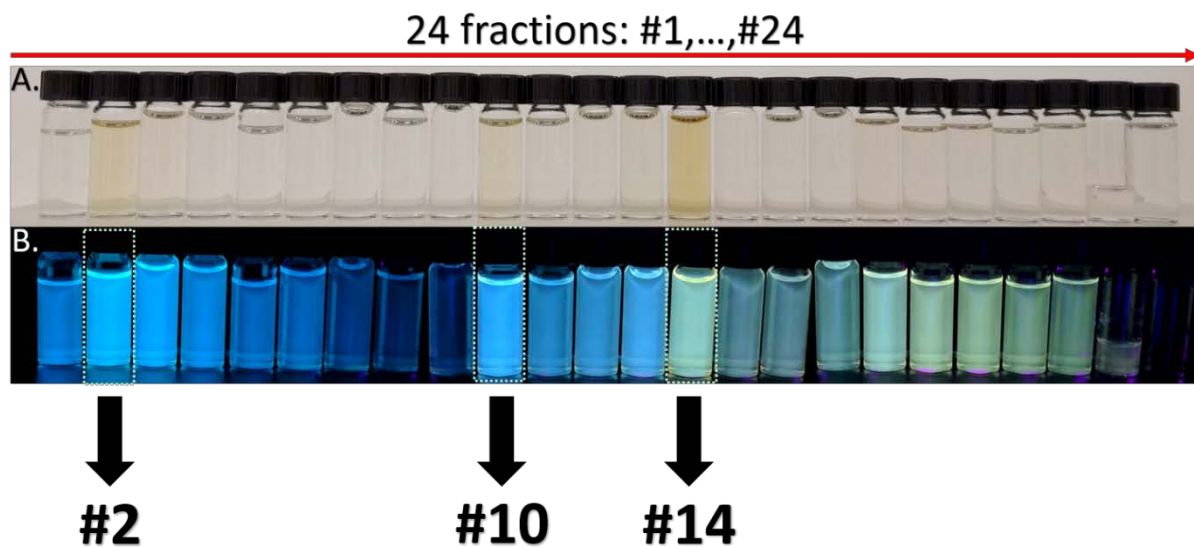


Figure S4. Photographic images of MACD fractions after the first round of separation: (A) under room light and (B) under 365 nm UV lamp.

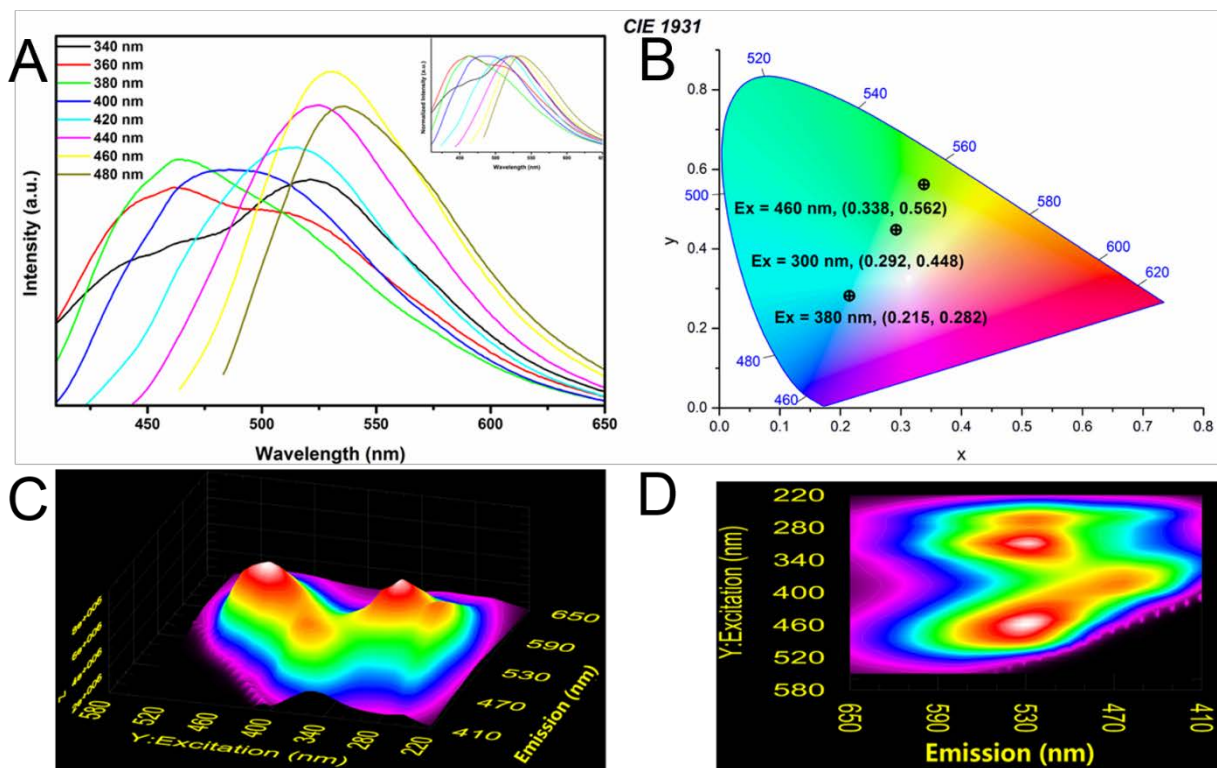


Figure S5. Fluorescence properties of MACD fraction #14 after the first round of separation: (A) excitation-dependent emission, inset: normalized spectra, (B) CIE 1931 coordinates, (C) 3D excitation-emission matrix (EEM), and (D) 2D EEM.

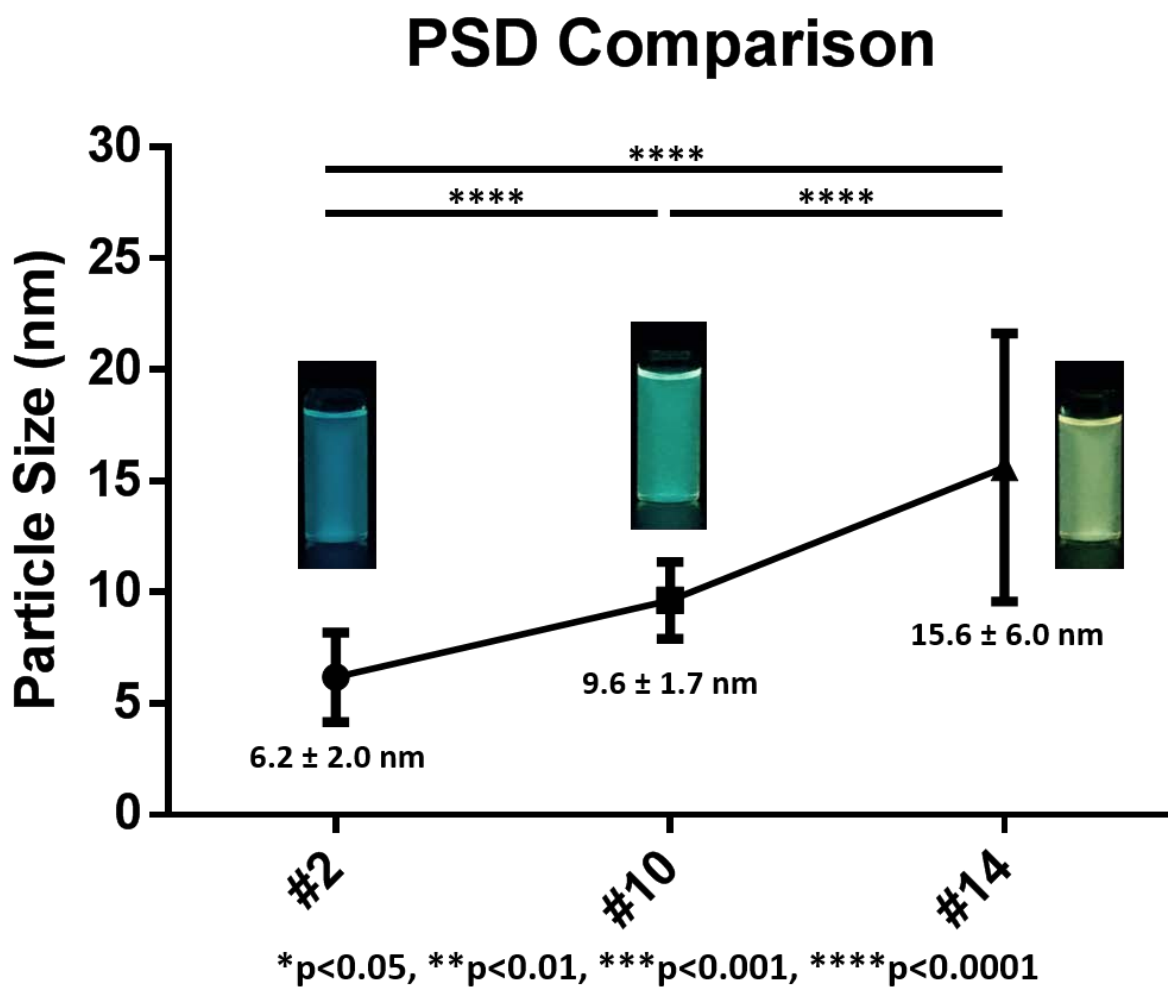


Figure S6. Significance test of the MACD fraction TEM PSDs.

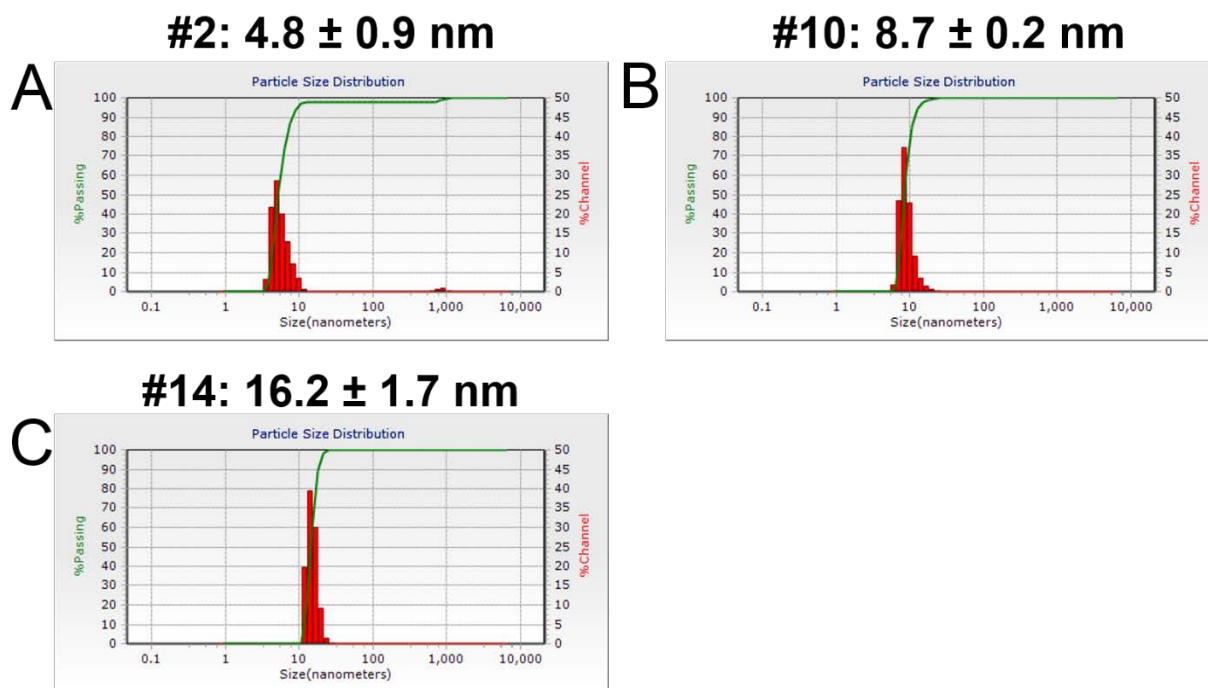


Figure S7. MACD fraction DLS: PSD of fraction (A) #2, (B) #10, and (C) #14.

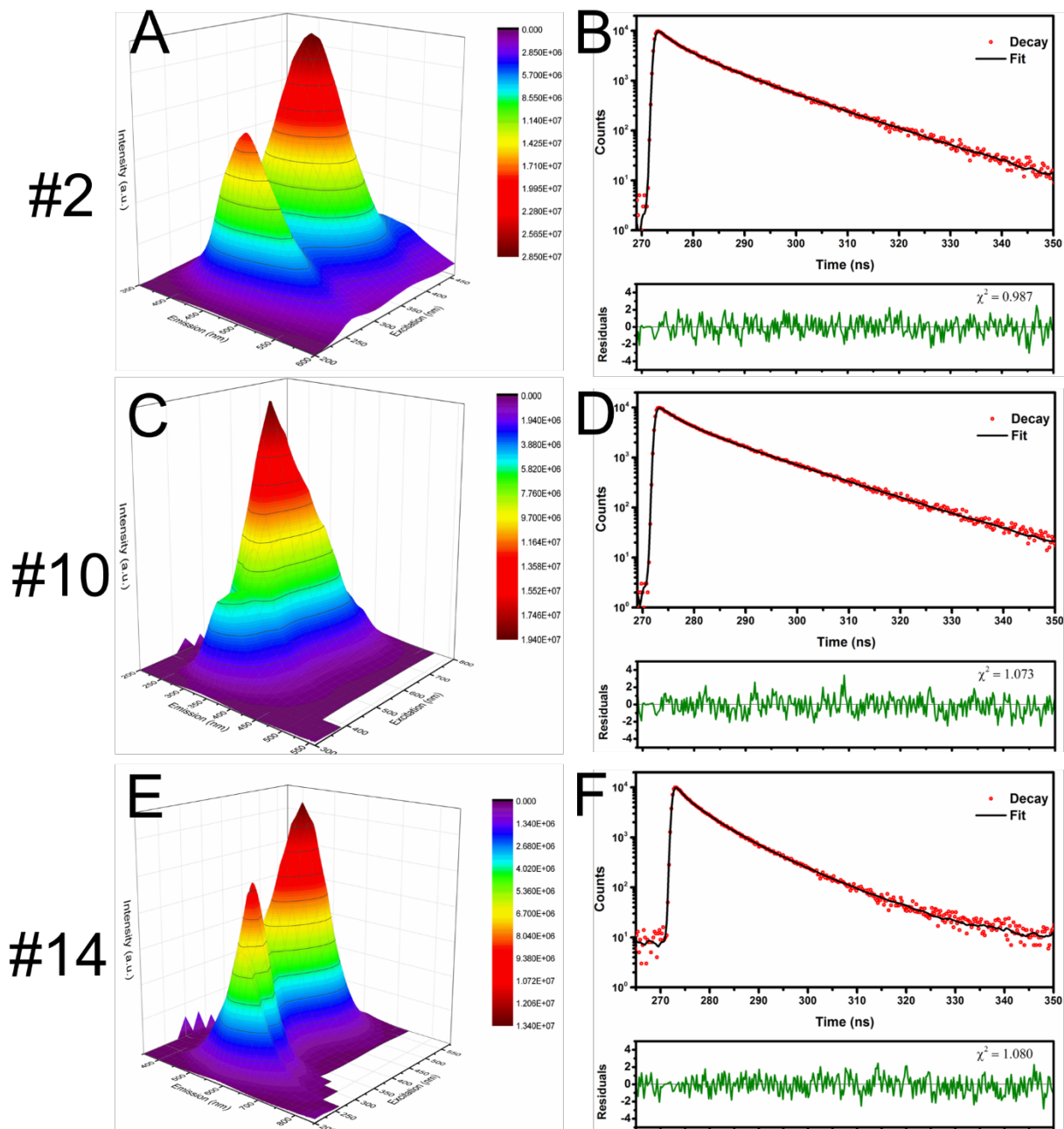


Figure S8. Upper panel: (A) 3D EEM and (B) fluorescence decay traces of MACD fraction #2; middle panel: (C) 3D EEM and (D) fluorescence decay traces of MACD fraction #10; lower panel: (E) 3D EEM and (F) fluorescence decay traces of MACD fraction #14.

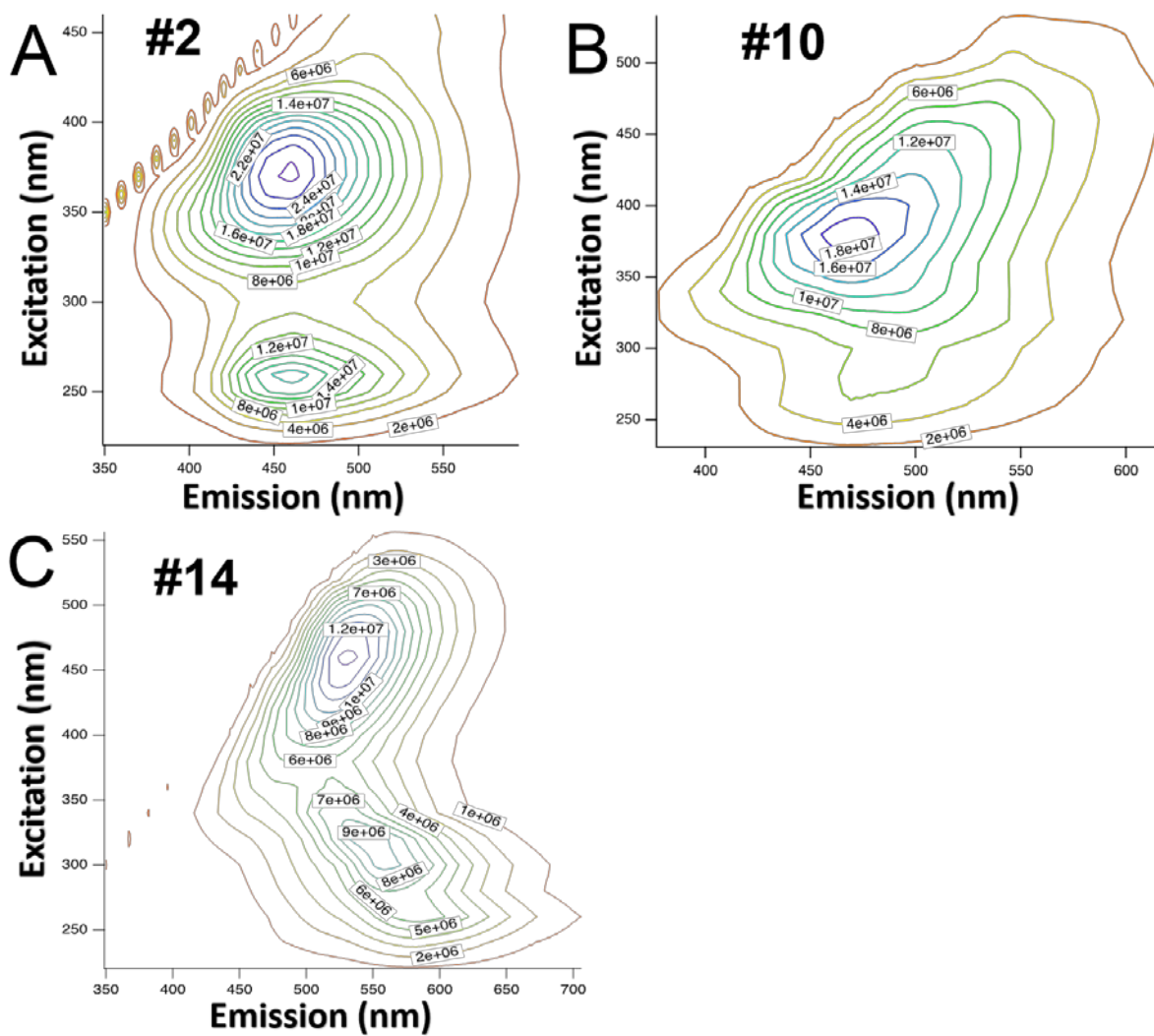


Figure S9. 2D excitation emission contour images of MACD fractions: (A) #2, (B) #10, and (C) #14.

CCTCCTTCATAGCACGTTTG
ACTTGGTCTTCTTACTGGCC
TCTCATCGTCACTCACAGCA
CCTCGAATCTGAAGAGTGTA
TCACTCAGTTCAAGACTGTC
ATTTGTCAGCGTCGGCAACA
TTGGTGAGGCATTTCTGACG
CTTCACCAGTAGTTTCTTCC
TCAGTCAGAGTCGCTCTTCT
ATGGAACCGAATCTCGCTCT
GTGTCATGGCTTGCTGAAAT
CTACCGGTTTCCAACCTATAG

Table S1: Oligonucleotide sequences used as probes for p53 smFISH. Each probe was labeled with Alexa647.